# Mechanistic Studies of an Unusual Amide Bond Scission

**Christopher J. Creighton, Todd T. Romoff,† Jane H. Bu, and Murray Goodman***

*Contribution from the Department of Chemistry and Biochemistry, University of California at San Diego, La Jolla, California 92093-0343*

*Received April 23, 1999*

**Abstract:** Unusual acid cleavage reactions are reported for derivatives containing acylated *N*-methyl-α-aminoisobutyryl (*N*MeAib) residues. The bond linking the *N*MeAib residue to the following amino acid is cleaved. Through X-ray diffraction studies of the *N*MeAib containing molecules, we have shown that the carbonyl oxygen atom of the preceding residue is in proximity to the carbonyl carbon of the *N*MeAib residue. Thus, it can act as an internal nucleophile leading to a cleavage reaction by way of an oxazolinium ion intermediate. Kinetic experiments for the cleavage reaction were carried out on a series of benzoyl dipeptide derivatives (*p*-X-$C_6H_4C$(O)-*N*MeAib-Phe-OMe) where X is varied from $NO_2$ to Cl. The value of $\rho = -1.335$ for the Hammett linear free-energy relationship strongly supports the intermolecular oxazolinium intermediate proposed.

## Introduction

Recently, we reported[1,2] an unusual reaction during the deprotection of the cyclic hexapeptide somatostatin analogue c[Phe-DTrp-Lys(Boc)-Thr(tBu)-Phe-*N*MeAib] (**1**) (where *N*MeAib denotes an *N*-methyl-α-aminoisobutyryl residue). Upon treatment of compound **1** with TFA and 1,2-ethanedithiol, two linear deprotected hexapeptides were obtained: H-Phe-DTrp-Lys-Thr-Phe-*N*MeAib-OH (**2**) and its C-terminal 2-thioethyl thioester (**3**) (Figure 1). Since peptides are routinely treated with strong acids such as TFA and anhydrous HF without loss of backbone integrity, this facile amide bond cleavage[3−9] is most unusual. To investigate this amide bond cleavage reaction, we synthesized peptides containing *N*MeAib residues. Crystallographic studies were carried out on several of the *N*MeAib peptides. The crystal structures were examined for possible steric evidence to explain the lability of the amide bond between the *N*MeAib residue and the adjacent amino acid in these peptides. No unusual bond geometries were observed. The peptides were then subjected to acidic conditions and their rates of acidolysis determined. From these two studies, we concluded that the mechanism for cleavage of this amide bond occurs via an oxazolinium ion intermediate[10,11] and not from the conventional AAC2 mechanism.[12,13]

## Results and Discussion

**Cleavage Studies using c[Phe-Ser(Bn)-Ser(Bn)-Phe-*N*MeAib] (4).** An investigation of the properties of cyclic pentapeptide **4** revealed that it also cleaves (Figure 2) specifically at the *N*MeAib-Phe bond in neat TFA ($t_{1/2} = 2.0$ h) to give the linear pentapeptide H-Phe-Ser(Bn)-Ser(Bn)-Phe-*N*MeAib-OH (**5**).

We carried out kinetic experiments for the acidolysis of c[Phe-Ser(Bn)-Ser(Bn)-Phe-*N*MeAib] (**4**). The TFA-mediated acidolysis of c[Phe-Ser(Bn)-Ser(Bn)-Phe-*N*MeAib] is pseudo-first-order with respect to the peptide. This is demonstrated by the linear relationship shown in Figure 3B.

We also examined how solvent and acid concentrations influence the rate of acidolysis (Table 1). The reaction rate decreases by addition of water. Solvent polarity has a strong influence on the rate of cleavage, as shown by acidolysis of **4** in 1:1 TFA:$CH_3CN$ ($t_{1/2} = 1.1$ h) compared to cleavage in 1:1 TFA:$CH_2Cl_2$ ($t_{1/2} = 4.1$ h). Increasing the concentration of TFA in $CH_3CN$ increases the rate of scission.

**Crystallographic Study of c[Phe-Ser(Bn)-Ser(Bn)-Phe-*N*MeAib].** The ORTEP diagram of c[Phe-Ser(Bn)-Ser(Bn)-Phe-*N*MeAib] (**4**) is shown in Figure 4. This structure demonstrates that all of the amide bonds exhibit normal bond lengths and geometries.[14] The dihedral angles of the amide bonds range from 159.7 to −174.4°, and the C−N bond lengths range from 1.327 to 1.360 Å. The labile amide bond has a bond angle of −174.4° and a bond length of 1.345 Å. We carried out $^{13}C$ NMR studies of c[Phe-Ser(Bn)-Ser(Bn)-Phe-*N*MeAib]. Our studies reveal no unusual chemical shifts for the carbonyl carbons indicating all amides exhibit normal geometries in solution. Thus, these results indicate the sensitivity of the amide bond to acid does not arise

* To whom correspondence should be addressed.
† Current address: The Affymax Research Institute, Santa Clara, California 95051.

(1) Spencer, J. R.; Delaet, N. G. J.; Toy-Palmer, A.; Antonenko, V. V.; Goodman, M. *J. Org. Chem.* **1993**, *58*, 1635.
(2) Spencer, J. R.; Toy-Palmer, A.; Jiang, J. X.; Li, H.; Tran, T.-A.; Romoff, T. *Proc. 13th Am. Peptide Symp*. **1994**, Edmonton (Hodges, R. S., Smith, John A., Eds.) pp 211−214, ESCOM, Leiden.
(3) Bender, M. L. *Chem. Rev.* **1960**, *60*, 53.
(4) Bromilow, J.; Abboud, J. L. M.; Lebrilla, C. B.; Taft, R. W.; Scorrano, G.; Lucchini, V. *J. Am. Chem. Soc.* **1981**, *103*, 5448.
(5) Yates, K.; Modro, T. A. *Acc. Chem. Res.* **1978**, *11*, 190.
(6) Duffy, J. A.; Leinstein, J. A. *J. Chem. Soc.* **1960**, 853.
(7) Williams, A. *J. Am. Chem. Soc.* **1976**, *98*, 5645.
(8) Perrin, C. L. *Acc. Chem. Res.* **1989**, *22*, 268.
(9) Edwards, J. T.; Derdall, G. D.; Wong, S. C. *J. Am. Chem. Soc.* **1978**, *100*, 7023.
(10) Urban, J.; Vaisar, R. S.; Lee, M. S. *Int. J. Pept. and Protein Res.* **1996**, *47*, 1996.
(11) Proctor, P.; Gensmantel, N. P.; Page, M. I. *J. Chem. Soc. Perkin Trans. 2* **1982**, 1185.
(12) March, J. Aliphatic Nucleophilic Substitution. In *Advanced Organic Chemistry: Reactions, Mechanisms, and Structure*, 4th ed.; Wiley & Sons: New York, 1992; p 385.
(13) Lowery, T. H.; Richardson, K. S. Reactions of Carbonyl Compounds. In *Mechanism and Theory in Organic Chemistry*, 3rd ed.; HarperCollins: New York, 1987; p 720.
(14) Ramachandran, G. N.; Sasisekharan, V. Conformation of Polypeptides and Proteins. In *Advances in Protein Chemistry*; Anfinsen, C. B., Anson, M. L., Edsall, J. T., Richards, F. M., Eds.; Academic Press: New York, 1968; pp 283−438.

10.1021/ja9913131 CCC: $18.00 © 1999 American Chemical Society
Published on Web 07/14/1999

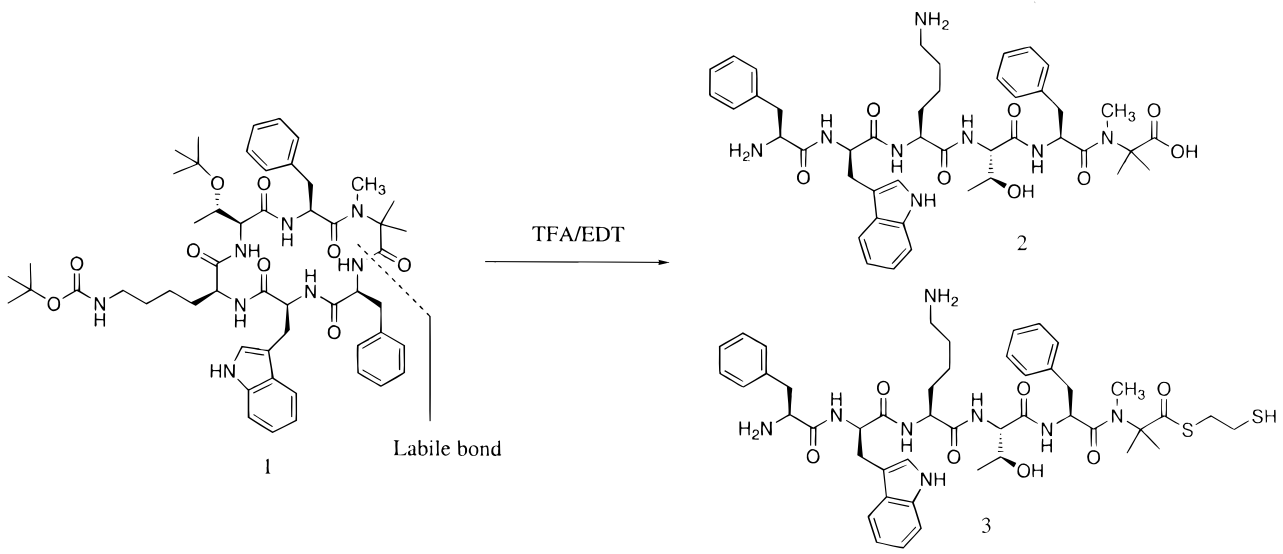


**Figure 1.** Acidolysis of c[Phe-DTrp-Lys(Boc)-Thr(tBu)-Phe-*N*MeAib] (**1**).

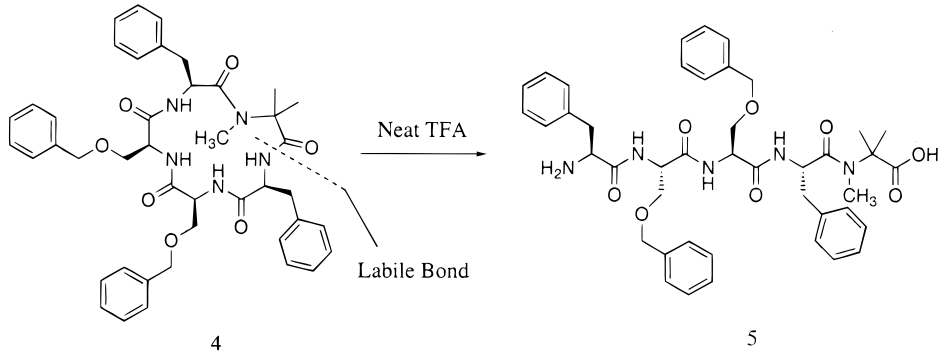


**Figure 2.** Acidolysis of c[Phe-Ser(Bn)-Ser(Bn)-Phe-*N*MeAib] (**4**).

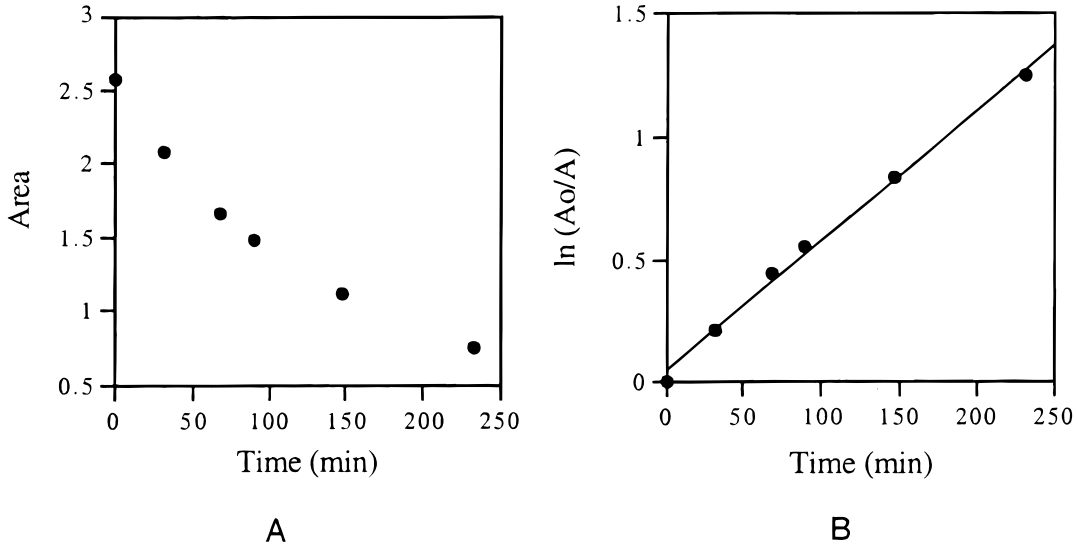


**Figure 3.** The acidolysis of c[Phe-Ser(Bn)-Ser(Bn)-Phe-*N*MeAib] (**4**) in neat TFA. The integrated area of c[Phe-Ser(Bn)-Ser(Bn)-Phe-*N*MeAib] (**4**) is plotted versus time in Figure 3A. The plot of $\ln(A_0/A)$ as a function of time is graphed in Figure 3B. The slope of the line in 3B indicates the rate constant for the reaction.

from distorted amide geometry.[15] The proximity (2.661 Å) of O4 and C35 can be seen in Figure 4. This orientation suggests that O4 may function as an internal nucleophile that leads to the tetrahedral transition state required for the scission of the amide bond.

(15) Shao, H.; Jiang, X.; Gantzel, P.; Goodman, M. *Chem. Biol.* **1994**, 231.

**The Study of Model Peptides Containing *N*MeAib.** We synthesized and obtained X-ray diffraction structures for compounds **6** and **7** (Figure 5). Kinetic studies of acidolysis were then carried out on these molecules. The ORTEP diagrams of peptides **6** and **7** (Figure 6) show constrained turns induced by the *N*MeAib residues with O1 in close proximity to C11 in both cases (2.69 Å for **6** and 2.61 Å for **7**). For all cases where

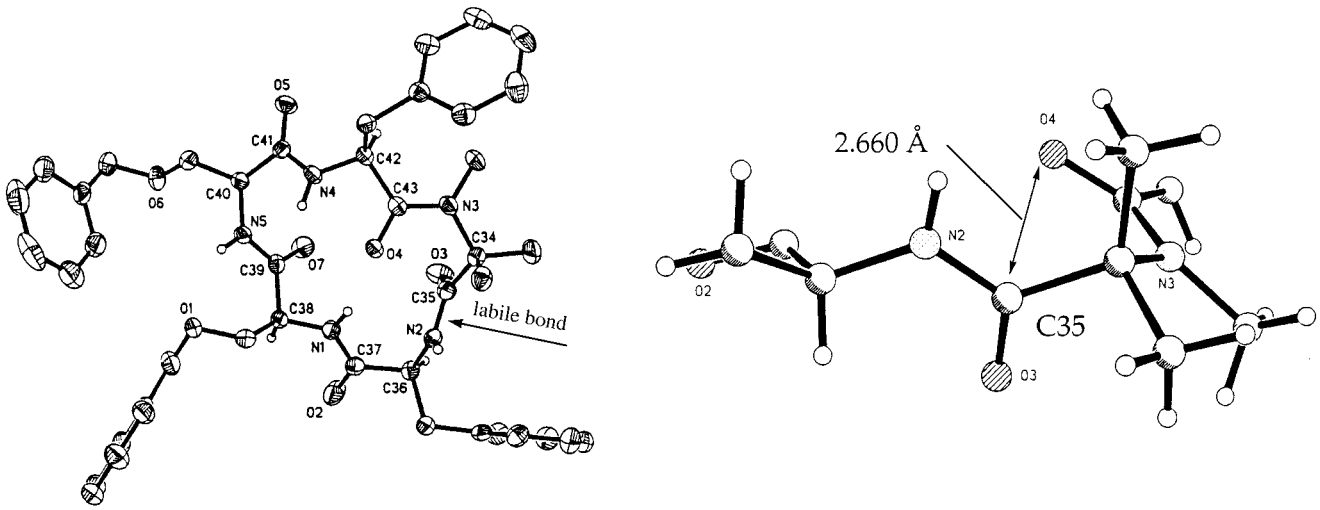


**Figure 4.** The ORTEP diagram of c[Phe-Ser(Bn)-Ser(Bn)-Phe-*N*MeAib] (**4**) and the distance geometry of O4 to C35.

**Table 1.** Acidolysis of c[Phe-Ser(Bn)-Ser(Bn)-Phe-*N*MeAib] (**4**)

| TFA (%) | solvent | $t_{1/2}$ (h) |
|---|---|---|
| 100 | neat | 2.0 |
| 95 | $H_2O$ | 8.0 |
| 50 | $CH_2Cl_2$ | 4.1 |
| 50 | $CH_3CN$ | 1.1 |
| 25 | $CH_3CN$ | 1.3 |
| 10 | $CH_3CN$ | 2.7 |

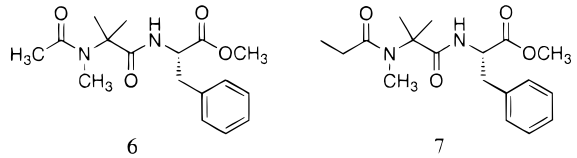


**Figure 5.** Dipeptide derivatives containing an *N*MeAib residue. Ac-*N*MeAib-Phe-OMe (**6**) and Pr-*N*MeAib-Phe-OMe (**7**).

we have obtained X-ray diffraction structures for *N*MeAib peptides, we observed the oxygen of the preceding carbonyl to be in close proximity to the carbon on the Aib carbonyl.

The rate of cleavage (Figure 7) was measured for compounds **6** and **7** in 1% TFA/$CH_3CN$. Figure 7A shows the integrated area (A) of the HPLC trace for dipeptide derivatives **6** and **7** as a function of time. In Figure 7B the $\ln(A_0/A)$ is plotted as a function of time for each peptide where ($A_0$) is the initial area of the peptide at time zero. The linear relationships indicate pseudo-first-order reactions in which the slope is the rate constant for acidolysis.[16] Both peptides, **6** and **7**, are much more sensitive to TFA than the highly constrained cyclopentapeptide **4**. The rate constant of cleavage for Ac-*N*MeAib-Phe-OMe (**6**) is $0.53 \times 10^{-3}$ s$^{-1}$ and for Pr-*N*MeAib-Phe-OMe (**7**) $1.11 \times 10^{-3}$ s$^{-1}$. Compound **6** cleaves twice as fast as compound **7** in 1% TFA:$CH_3CN$.

**Proposed Mechanism for Acidolysis of *N*MeAib Peptides.** As indicated in Scheme 1, we propose that the mechanism for acidolysis proceeds via an intramolecular tetrahedral intermediate. Once the tetrahedral intermediate is formed, the lone-pair electrons on the nitrogen of phenylalanine are no longer in conjugation with the carbonyl $\pi$-bond of *N*MeAib. As an amine-like structure, the phenylalanine nitrogen becomes a proton acceptor. Thus, phenylalanine is ejected, and the system collapses to an oxazolinium ion intermediate[4] that immediately reacts with trace water to form the carboxylic acid product.

To assess the effectiveness of the acetyl oxygen as an internal nucleophile, we synthesized a series of benzoyl dipeptides and determined their rate of acidolysis using 2% TFA in $CH_3CN$ (Figure 8). The kinetics of cleavage for these para-substituted benzoyl dipeptides are summarized in Figure 9. The reactions of *p*X-$C_6H_4$C(O)-*N*MeAib-Phe-OMe with 2% TFA in acetonitrile display pseudo-first-order kinetics (Table 2). The plots of $-\ln(A)$ versus time is linear with the slopes equal to the rate constants for acidolysis. The change in rates for the series *p*X-

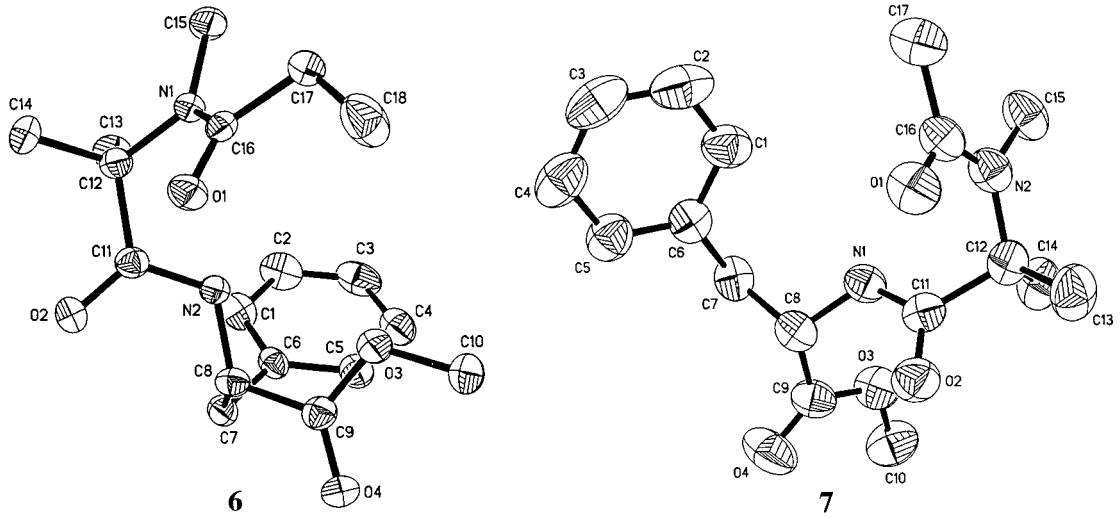


**Figure 6.** ORTEP diagram of Ac-*N*MeAib-Phe-OMe **6** and Pr-*N*MeAib-Phe-OMe **7**.

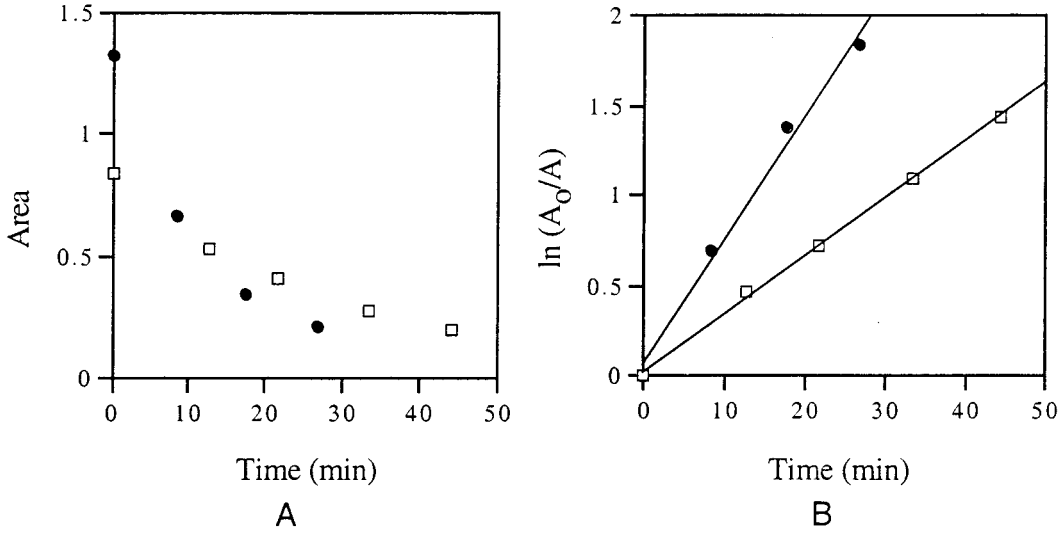


**Figure 7.** Acidolysis of peptides **6** and **7** in 1% TFA/$CH_3CN$. In Figure 7A the integrated area of the peptides is plotted versus time where □ denotes Ac-*N*MeAib-Phe-OMe (**6**) and ● Pr-*N*MeAib-Phe-OMe (**7**). In Figure 7B the ln($A_0$/*A*) is graphed versus time for the acidolysis of each peptide. The slope of each line indicates the rate constant for each reaction.

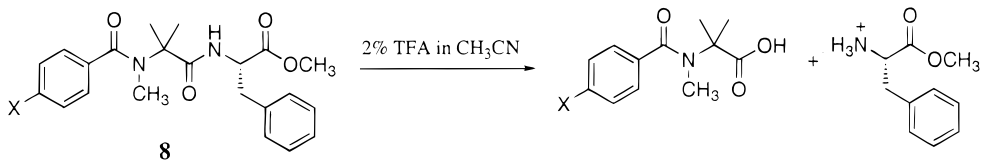


**8**

**8a X= $NO_2$**
**8b X= CN**
**8c X= $CF_3$**
**8d X= Cl**
**8e X= $CH_3$**

**Figure 8.** Acidolysis of *p*X-$C_6H_4C$(O)-*N*MeAib-Phe-OMe with 2% TFA in $CH_3CN$.

**Scheme 1**

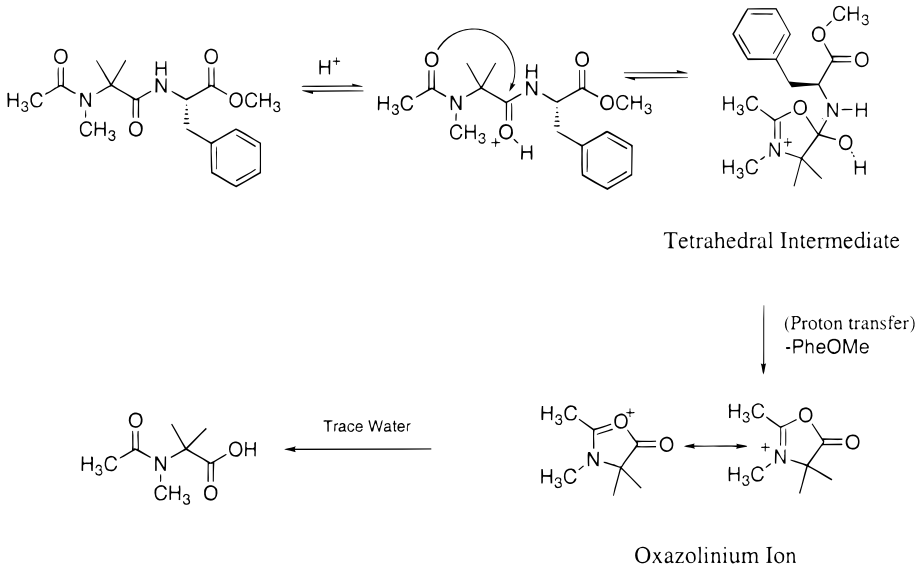


$C_6H_4C$(O)-*N*MeAib-Phe-OMe is a function of the electronic effects of the substituents, specifically, their electron-donating or electron-withdrawing nature.[17] The remote proximity of the X group allows for a constant steric environment about the reaction center.

**Hammett Equation Applied to Acidolysis of *p*X-$C_6H_4C$-(O)-*N*MeAib-Phe-OMe Peptides.** The Hammett equation (eq 1) was used to solve for $\rho$ by plotting log *k* versus $\sigma$.

$$\log k = \rho\sigma + \log k_0 \qquad (1)$$

The variable *k* is the rate constant for acidolysis of the para-substituted dipeptide (compounds **8a**−**d**) and $k_0$ is the rate constant for the unsubstituted benzoyl dipeptide. The substituent

(16) March, J. Mechanisms and the Methods of Determining Them. In *Advanced Organic Chemistry: Reactions, Mechanisms, and Structure*, 4th ed.; Wiley & Sons: New York, 1992; p 220−224.
(17) Hammett, L. P. *J. Am. Chem. Soc.* **1937**, *59*, 96.

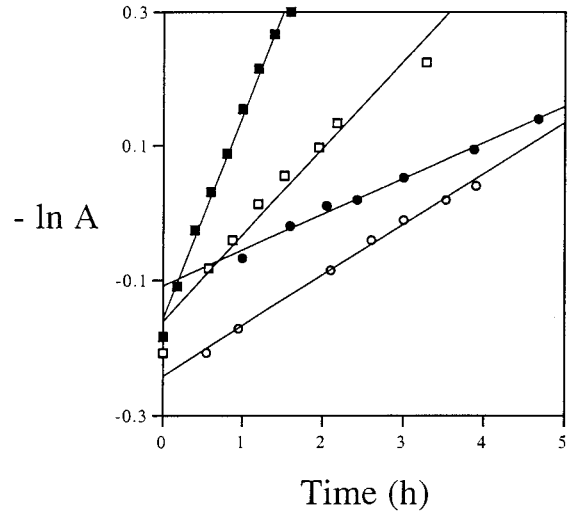


**Figure 9.** Plots of $-\ln(A)$ versus time for the acidolysis of $p$X-$C_6H_4$C-(O)-*N*MeAib-Phe-OMe in 2% TFA/$CH_3CN$ where Cl (■), X = $CF_3$ (□), CN (○) and $NO_2$ (●). The slope of each line indicates the rate constant for the acidolysis of each derivative.

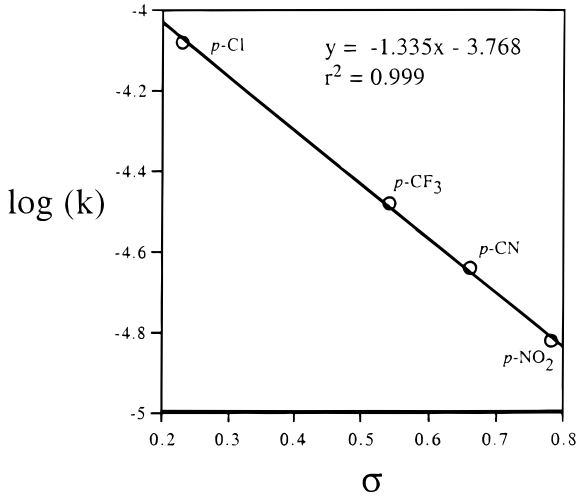


**Figure 10.** The log k is plotted versus $\sigma$ for the cleavage of $p$X-$C_6H_4$C-(O)-*N*MeAib-Phe-$OCH_3$ in 2% TFA in $CH_3CN$.

constant, $\sigma$ is defined by eq 2.

$$\sigma = \log(K_a/K_0) \qquad (2)$$

Where $K_a$ is the dissociation constant for each para-substituted benzoic acid and $K_0$ is the dissociation constant of benzoic acid.[18] The magnitude and sign of $\rho$ reflects the geometry of the transition state[17,19,20] and indicates the influence of the para substituents on the remote reaction center. Since the rate constant values for all of the substituents fall on a single line (Figure 10), we conclude that there is no change in the mechanism over the series of benzoyl dipeptides studied. The linearity of Figure 10 demonstrates that a linear free-energy relationship[22,23] exists among the acids and the peptides with $\rho = -1.335$.

**Table 2.** Acidolysis of $p$X-$C_6H_4$C(O)-*N*MeAib-Phe-OMe with 2% TFA in acetonitrile

| compd | $k$ ($s^{-1}$) | $t_{1/2}$ (h) | $\sigma$ |
|---|---|---|---|
| $NO_2$ | $1.5 \times 10^{-5} \pm 0.1 \times 10^{-5}$ | 12 | 0.78 |
| CN | $2.3 \times 10^{-5} \pm 0.1 \times 10^{-5}$ | 8 | 0.66 |
| $CF_3$ | $3.7 \times 10^{-5} \pm 0.2 \times 10^{-5}$ | 5 | 0.54 |
| Cl | $8.3 \times 10^{-5} \pm 0.3 \times 10^{-5}$ | 2 | 0.23 |
| $CH_3$ | too fast to determine by HPLC | | −0.17 |

The observation that $\rho$ is large and negative supports the contention that the substituents at the para-position have a significant electronic effect at the remote reaction center. Electron-donating substituents increase the reaction rate, while electron-withdrawing substituents slow the reaction. The magnitude of $\rho$ provides valuable insight into the effect of the para-substituents on the remote reaction center. If the acid-catalyzed reaction of our dipeptide derivatives were to proceed through a conventional AAC2 mechanism (with water or trifluoroacetate acting as a nucleophile), the expected value for $\rho$ would be much smaller than −1.335.[17,19−24] The magnitude and sign of $\rho$ indicate that the carbonyl oxygen of the benzoyl group is intimately involved in the transition state for the rate-determining step. The results strongly support an intramolecular oxazolinium ion mechanism for acid-catalyzed cleavage of peptides containing *N*MeAib.

## Experimental Section

**General Procedure for Kinetic Studies.** Powdered $p$-CN-$C_6H_4$(O)-*N*MeAib-Phe-OMe (0.010 g, 0.025 mmol) was added to a flame-dried 10-mL round-bottom flask. To this solid, a solution of naphthalene (the internal standard) in acetonitrile (0.980 mL, 0.5 mg/mL) was added via a syringe. The solution was allowed to stir at room temperature until all of the dipeptide dissolved. After approximately 20 min, pure TFA (0.020 mL) was added to the reaction vessel. Immediately, an aliquot (0.010 mL) of the reaction mixture was removed with a syringe and added to scintillation vial containing 0.090 mL of pure acetonitrile (quench = $t_0$). From the scintillation vial 0.010 mL of the quenched solution was removed with a syringe and injected on the HPLC. Typically we observed an injection peak at 2.5 min, $p$-CN-$C_6H_4$(O)-*N*MeAib-OH at 3 min, dipeptides between 4 and 8 min, and naphthalene at 8.5 min. Aliquots were removed, quenched, and injected approximately every 30 min. Kinetic studies (HPLC) were carried out on a Waters M-6000 pump using a Vydac C18 (218TP54) column and a Kratos spectraflow 757 UV detector (210 nm). The isocratic mobile phase was composed of 50/50 acetonitrile/water for all kinetic HPLC experiments. All data were entered in an Excel spreadsheet and analyzed using the Analysis Tool Pack Regression Set to obtain rate constants.

**X-ray Diffraction Studies.** Data were collected with a Siemens R3m/V diffractometer (Mo K$\alpha$ $\lambda$ = 0.71073 Å). Direct methods revealed all of the non-hydrogen atoms for compounds **4**, **6**, and **7**. All non-hydrogen atoms were refined anisotropically for compounds **4**, **6**, and **7**, and the final least-squares refinement for each structure converged at the *R*-factors reported in Table 3. All calculations were preformed using SHELXTL PLUS programs. Full crystollographic details for compounds **4**, **6**, and **7** have been provided in the Supporting Information.

(18) Hansch, C.; Leo, A.; Unger, S. H.; Kim, K. H.; Nikaitani, D.; Lien, E. J. *J. Med. Chem.* **1973**, *16*, 7.
(19) Dippy, J. F. J.; Page, J. E. J. *J. Chem. Soc.* **1938**, 357.
(20) Jaffe, H. H. *J. Chem. Phys.* **1953**, 415.
(21) Stecher, E. D.; Ryder, F. H. *J. Am. Chem. Soc.* **1952**, 4392.
(22) Lowry, T. H.; Richardson, K. S. Some Fundamentals of Physical Organic Chemistry. In *Mechanism and Theory in Organic Chemistry*, 3rd ed.; HarperCollins: New York, 1987; p 143.
(23) March, J. Effects of Structure On Reactivity. In *Advanced Organic Chemistry: Reactions, Mechanisms, and Structure*, 4th ed.; Wiley & Sons: New York, 1992; pp 278−286.
(24) Jaffe, H. H. *Chem. Rev.* **1953**, *53*, 191.
(25) Hammett reports $\rho = +0.118$ for acidolysis of substituted benzamides in ref 17. It has been shown that insertion of methylene groups between $p$X-$C_6H_4$ and the reaction site COOR attenuates $\rho$ by $^1/_2$ for each methylene group. Thus for $p$X-$C_6H_4$COOH $\rho = 1$, for $p$X-$C_6H_4CH_2$COOH $\rho = 0.489$, and for $p$X-$C_6H_4CH_2CH_2$COOH $\rho = 0.212$. See ref 22 pp 144−147.

**Table 3.** Crystal Data and Structure Refinement for c[Phe-Ser(Bn)-Ser(Bn)-Phe-*N*MeAib] (**4**), Ac-*N*MeAib-Phe-OMe (**6**), and Pr-*N*MeAib-Phe-OMe (**7**)

| | **4** | **6** | **7** |
|---|---|---|---|
| empirical formula | $C_{43}H_{49}N_5O_7$ | $C_{17}H_{24}N_2O_4$ | $C_{18}H_{26}N_2O_4$ |
| formula weight | 747.89 | 320.38 | 334.41 |
| temperature (K) | 169 | 299 | 188 |
| crystal system | triclinic | monoclinic | monoclinic |
| space group | *P*1 | $P2_1$ | $P2_12_12_1$ |
| unit cell dimensions | | | |
| *a* (Å) | 6.243 | 9.524 | 9.625 |
| *b* (Å) | 13.270 | 9.981 | 9.634 |
| *c* (Å) | 13.387 | 9.621 | 10.396 |
| $\beta$ (deg) | 77.05 | 108.07 | 114.13 |
| volume (Å$^3$) | 989.9 | 869.4 | 879.8 |
| *Z* | 1 | 2 | 2 |
| density (mg/mm$^3$) | 1.255 | 1.224 | 1.262 |
| absorption coefficient (mm$^{-1}$) | 0.086 | 0.087 | 0.089 |
| F (000) | 398 | 344 | 360 |
| crystal size (mm) | 0.075 × 0.15 × 1.00 | 0.50 × 0.60 × 0.90 | 0.50 × 0.40 × 0.30 |
| crystal color | colorless acicular | colorless | colorless |
| $\theta$ range for data collect. (deg) | 1.5 to 25 | 1.5 to 27.5 | 2.15 to 27.49 |
| limiting indices | | | |
| | $0 \le h \le 7$ | $0 \le h \le 12$ | $0 \le h \le 12$ |
| | $-15 \le k \le 15$ | $0 \le k \le 12$ | $0 \le k \le 12$ |
| | $-15 \le l \le 15$ | $-12 \le l \le 11$ | $-13 \le l \le 12$ |
| reflections collected | 3837 | 2212 | 2196 |
| independent reflections | 3837 | 2104 | 2100 |
| refinement method | full matrix least-squares on $F^2$ | full matrix least-squares on $F^2$ | full matrix least-squares on $F^2$ |
| data/restraints/parameters | | | 2100/1/222 |
| goodness of fit on $F^2$ final *R* indices | 1.31 | 1.49 | 1.046 |
| R1 | 3.53 | 3.97 | 0.0573 |
| wR2 | 5.04 | 5.95 | 0.1467 |
| *R* indices (all data) | | | |
| R1 | 3.84 | 4.64 | 0.0727 |
| wR2 | 5.13 | 6.16 | 0.1627 |

**Acknowledgment.** We thank Dr. Peter Gantzel (UCSD) for the X-ray crystallographic studies, Dr. Gary Siuzdak from The Scripps Research Institute for mass spectrometry analysis, The Affymax Research Institute for funding, and Prof. Charles Perrin (UCSD) for his insightful discussions about kinetics and mechanisms.

**Supporting Information Available:** We have provided detailed descriptions of the syntheses of compounds **4**, **6**, **7**, and **8a**−**d** including elemental analysis, analytical HPLC, optical rotation, melting points, and high-resolution mass spectrometry. X-ray crystallographic data is provided for compounds **4**, **6**, and **7**. We also included tables of the data for acidolysis of compounds **8a**−**d** in TFA:$CH_3CN$ (PDF). This material is available free of charge via the Internet at http://pubs.acs.org.

JA9913131